# Observations of Stratospheric Gravity Waves During the WB57F Aerosol Mission and Modeling with Mesoscale Model 5

Jeffrey Hicke[1,2,3]

Karen Rosenlof[2,3]

Adrian Tuck[2]

M. J. Mahoney[4]

Susan Hovde[2,3]

[1] PAOS, University of Colorado, Boulder

[2] NOAA Aeronomy Lab, Boulder, Colorado

[3] CIRES, University of Colorado, Boulder

[4] Jet Propulsion Laboratory, Pasadena, California

DRAFT

April 5, 2000

To be submitted to the

*Journal of the Atmospheric Sciences*

## Abstract

On April 11, 1998 the WB57F aircraft flew northwest at lower stratospheric altitudes from Houston, Texas, over eastern Wyoming as part of the WB57F Aerosol Mission to sample a vortex filament forecast to pass over that region. Observations of meteorological quantities as well as ozone, water vapor, and aerosols confirm the presence of vortex air during the flight, though the source of the vortex air is inconclusive from trajectory modeling. Severe turbulence was reported by the pilot in the lower stratosphere over Wyoming and the measurements of horizontal winds, ozone, and profiles of temperature on board indicate breaking gravity waves. The NCAR/Penn State Mesoscale Model 5 (MM5) was run to assess its capability of reproducing the gravity waves. The model successfully simulated the occurrence of the waves, though the vertical extent is more limited than the observations and in one case the intensity was somewhat less than the observations. Scaling properties were computed to demonstrate quantitatively that the MM5 output is smoother than the observations at wavelengths significantly larger than the model resolution. Both the temperatures and the horizontal winds scale differently between the model and the observations. The model output tends toward persistence (or correlation) while the observations tend toward antipersistence (or anticorrelation). The model output lacks the small scale structure in both winds and temperature seen in the observations and so may be deficient in modeling the behavior of the atmosphere at scales below 50 km despite a grid spacing of 6.67 km.

## 1. Introduction

Gravity waves influence the stratosphere through a number of processes. During winter in the polar vortices, air lifted by gravity waves can cool enough adiabatically to reach frost point temperatures and form polar stratospheric clouds, and thus may play an important role in ozone depletion. Breaking gravity waves exert a drag on the circulation in the stratosphere and are important for jet stream simulation near the tropopause in numerical weather prediction models; some representation of gravity waves is needed in general circulation models to accurately simulate the dynamics in the middle atmosphere. Breaking gravity waves also cause convective instabilities in the atmosphere as potential temperature ($\theta$) surfaces become vertical, mixing air and constituents vertically as a result. In addition, breaking gravity waves generate severe turbulence in the troposphere and stratosphere that could damage aircraft.

Few simulations of stratospheric gravity waves using aircraft observations have been reported in previous studies, though these observations are needed to help assess the modeling capabilities of gravity waves. Bacmeister et al. (1990) used a linear model to simulate a gravity

wave observed by the ER-2 over Antarctica. Leutbecher and Volkert (1996) discussed modeling a gravity wave with the NCAR/Penn State University Mesoscale Model version 5 (MM5) (Grell et al. 1994), but did not have observations for comparison.

The WB57F Aerosol Mission was designed to sample the upper troposphere and lower stratosphere with a variety of aerosol, trace gas, and meteorological instruments. On April 11, 1998, the WB57F flew northwest from Houston, Texas (30°N, 95°W) toward the forecast location of a filament of air that had recently peeled off of the polar vortex. While over central Wyoming (42°N, 105°W) the pilot reported severe turbulence at lower stratospheric altitudes indicative of breaking gravity waves. The severe turbulence encountered by the aircraft was collocated with a blob of high potential vorticity (PV) seen in the European Center for Medium Range Weather Forecasts (ECMWF) analyses at 450 K potential temperature surface. This high PV air may have originated from high latitudes in or around the polar vortex, and could have an influence on the propagation and breaking characteristics of gravity waves through a change in the static stability in the lower stratosphere.

This study analyzes the origin of the filament with observations from the WB57F together with trace gas observations from satellite and trajectory modeling. The gravity waves as recorded by aircraft instrumentation are discussed, and a modeling simulation of the region using MM5 is presented. The observations on board the WB57F are then compared to model results across a range of scales. Models simulating the atmosphere should accurately represent small as well as large scales, and comparison with observations allows the assessment of the model's accuracy. Power spectra and scaling invariance properties were computed to analyze model and observational data.

The paper is organized as follows. The next section describes the observations of the vortex filament and compares them with numerical weather prediction model analyses. It also analyzes the observations of the gravity waves. Section 3 describes the MM5 gravity wave modeling, while the section 4 presents the gravity wave modeling results. Section 5 compares the scaling behavior of the observations and model output, and conclusions are discussed in the final section.

## 2. Observations during WAM

The WB57F Aerosol Mission (WAM) occurred in spring 1998 and consisted of flights from Houston, Texas (30°N, 95°W) designed to study aerosols at middle and subtropical latitudes. Upper tropospheric and lower stratospheric altitudes were observed with a variety of aerosol (e.g., Murphy et al. 1998), trace gas (total water, ozone), and meteorological instruments (temperature,

pressure). Winds were not directly measured but inferred from aircraft motion and true heading using the aircraft's inertial navigation system (INS).

a. Vortex Air

On April 11, the WB57F flew northwest from Houston in an attempt to encounter air that had recently peeled off from the polar vortex. Figure 1 shows the ECMWF potential vorticity (PV) analyses for 18 UTC, about the time that the aircraft reached its turnaround point. The polar vortex was pushed off the pole over the dateline, and a long filament can be seen stretching across the highest latitudes down into the eastern Pacific Ocean. At mid-California (35°N) the filament bends eastward. A blob of high PV air along the flight track can be seen over eastern Wyoming (41°N, 105°W). This blob and a second over northeast New Mexico and northwestern Texas (36°N, 103°W) are apparently disjoint from the filament by several hundreds of km. The 20 PV unit contour (1 PV unit = $10^{-6}$ K $m^2$ $kg^{-1}$ $s^{-1}$) has been drawn on the map and is used to roughly indicate the location of the edge of the vortex. The PV blob in Wyoming was sampled by the WB57F, while the one in New Mexico was not. The aircraft was flying at approximately 400 K both north- and southbound over New Mexico, and the PV maps at 400 K do not show the anomalously high PV blob at that altitude. This is confirmed by the lack of evidence in the aircraft observations.

Figure 2 shows meteorological, trace gas, and aerosol observations on board the WB57F for the northernmost flight section. Figure 3 shows the map of the corresponding section of flight, with the letters "A" through "I" indicating the locations labeled in Figure 2. From Point "A" to Point "D", the flight was level in pressure at about 80 hPa but increasing in potential temperature from 430 to 450 K (Figure 1a) as a result of an increase in temperature (Figure 1b). Ozone during this time increased from 700 ppbv to above 2000 ppbv, and the fraction of aerosols with meteoritic content increased from 20–50% to 55–75% as measured by PALMS (Murphy et al. 1998) (Figure 1c). Water vapor was measured by two instruments on this flight. The JPL TDL [Reference ????] water vapor increased from less than 5 ppmv to about 6 ppmv from "A" to "D", while the NOAA water vapor increased from 4 to nearly 5 ppmv.

The signature of these observed quantities is suggestive of polar vortex air. The high ozone and high meteoritic fraction precludes a tropospheric source (Murphy et al. 1998). On only one other WAM flight did water vapor and ozone reach these high values above 430 K (May 6, 1998), and the high potential vorticity on that day also suggests that the aircraft flew through a possible remnant of vortex air. Ozone and water vapor profiles from the Halogen Occultation Experiment (HALOE) satellite instrument were used to further investigate this. Due to the orbit characteristics, HALOE observed only middle and lower latitudes during April 1998. Figure 4 shows the 12 HALOE profiles from April 8, 1998, and the map of their locations along with the

ECMWF potential vorticity at 450 K at 18 UTC. The profiles have a latitude range between 37 and 40°N. Using the 20 PV unit contour as an indicator of the vortex edge, all but one of the profiles are outside the vortex. The profile at 10°W longitude, plotted with a dashed curve in Figure 4a and a plus in Figure 4b, is located within a region of vortex air that has separated from the main vortex region which is pushed off the pole toward eastern Asia. The ozone and water vapor profiles at this location are clearly different from the other profiles at the same latitude.

There are systematic differences between the two water vapor measurements on board the WB57F (Figure 3d), and between those measurements and HALOE (reference ?????), so to "calibrate" the aircraft observations to the HALOE data the observations from early in the flight were compared to zonal mean HALOE values, excluding the vortex profile. Mean NOAA water vapor for this latitude range and between 410 and 435 K was 0.3 ppmv greater than HALOE values, and the mean JPL water vapor was 1.1 ppmv greater than HALOE. Subtracting these differences from the aircraft observations yields values around 4.5 ppmv. A similar analysis showed that the ozone measured on board the aircraft was slightly lower than the HALOE retrievals. The adjusted aircraft water vapor and ozone are plotted at 450 K in Figure 4a as the diamonds. Both are slightly lower at 450 K than the values from the HALOE profile within the vortex.

Animations of the ECMWF PV at 450 K backward in time from April 11 are inconclusive about the origin of the PV blob over Wyoming. It is not clear whether the blob recently peeled off of the long filament displayed in Figure 1 and was more rapidly advected to Wyoming than the filament itself, or peeled off from the vortex at an earlier time and a different location, or is simply a model anomaly. Back trajectories on the 450 K surface were run using the ECMWF analyses, initializing air parcels at 18 UTC on April 11 over a large region centered on Point "D". No trajectory showed clear evidence of coming from the vortex, though they passed close to the southern edge of the filament. Forward trajectories of parcels started on April 9 at 00 UTC within the large vortex filament seen over the eastern Pacific in Figure 1 do not approach closer than 1000 km of the aircraft flight track over Wyoming.

Thus, it appears from the intermediate trace gas observations on the aircraft compared to the HALOE profiles and the inconclusive evidence from the trajectories modeling that the WB57F most likely sampled air from the edge of the vortex. The analyses may not have the necessary spatial resolution to capture regions of high wind shear at the edge of the vortex, and so back trajectories would not be able to accurately estimate the path of air parcels from this region.

The blob of high PV air may have modified the atmospheric characteristics significantly and created a situation that allowed the severe turbulence reported by the WB57F pilot. Ertel's potential vorticity is defined as a product of the static stability and the absolute vorticity

$$PV = -g\,\partial\theta / \partial p\,(\zeta_\theta + f) \qquad (1)$$

where the relative vorticity is defined as

$$\zeta_\theta = \frac{\partial v}{\partial x} - \frac{\partial u}{\partial y} \qquad (2)$$

and is evaluated on a $\theta$ surface (Holton 1992). PV is a conserved quantity in the absence of friction and diabatic heating, and so the high PV blob over Wyoming could influence gravity wave propagation there through the modification of the static stability term. Breakdown of the ECMWF PV calculation revealed that the high PV blob over Wyoming was primarily a result of change in wind shear as manifested in the relative vorticity term, especially in $\partial u / \partial y$. The static stability term changed somewhat, but the magnitude of the change was not comparable to the change in wind shear. Further evidence regarding the possible role of the filament in the gravity wave breaking will be discussed in sections on the aircraft observations (section 2b) and MM5 modeling (section 4).

b. Gravity Waves

Over southeast Wyoming, labeled Point "D" in Figure 3, the pilot reported severe turbulence at about 75 hPa during the northbound section of the flight. The horizontal wind speed shows large fluctuations at that location, ranging from 0 to 25 m $s^{-1}$, and wind direction also reveals large swings (Figure 2e). Ozone measurements display increased variability during that time (Figure 2c).

The Microwave Temperature Profiler (MTP) (Denning et al. 1989) was on board the WB57F and measured temperature profiles every 15 seconds for a 14 km region centered on the aircraft altitude. The resulting $\theta$ surfaces along the flight track are plotted in Figure 5. At 62,600 s UTC (Point "D"), where the pilot reported severe turbulence, the potential temperature surfaces are nearly vertical. The accuracy of MTP is approximately 0.5 K of potential temperature near aircraft altitude; the accuracy decreases with distance away from the aircraft. Despite the larger absolute uncertainties at higher and lower altitudes, the shapes of the isentropes are accurate, and so these fluctuations are not a result of instrument errors.

The reports of severe turbulence by the pilot, the large fluctuations in wind and ozone, and the nearly vertical $\theta$ surfaces all are evidence of a breaking gravity wave. The location of the

gravity wave is just downstream of the Laramie Mountains (just south and west of Point "D" in Figure 3), which rise 500 m above the plain to the southwest. Prevailing near-surface winds were from the southwest at the time of the gravity wave observations as indicated by the 700 hPa ECMWF analyses at 18 UTC on April 11 (Figure 3). Thus, the observed gravity wave appears to have been generated by flow over topography and subsequently propagated to lower stratospheric altitudes.

Additional gravity waves can be seen in both the aircraft observations and in the MTP $\theta$ surfaces. Features at Point "I" in Figures 2, 3, and 5 also show evidence of gravity wave activity with increased variability in ozone, wind speed and direction, and sharp changes in the MTP $\theta$ surfaces. From the MTP cross-section the amplitude of the wave grows and the isentropes steepen with altitude above the aircraft. This location is downstream from the Bighorn Mountains, which rise 1500 m above the surrounding terrain.

The MTP temperature profiles can be used to compute the static stability term $-g\,\partial\theta / \partial p$ used in the PV calculation, though at a much higher vertical and horizontal resolution than the ECMWF analyses. At 450 K the static stability has slightly higher values near Point "D" (near aircraft level) and much higher values just before Point "F" (above aircraft level); this can be seen in Figure 5 as the compression of the isentropes. These regions of high static stability may be related to the high PV blob seen in the ECMWF analyses and vortex signature of aircraft observations at Point "D". At and before Point "F", there are spikes of high ozone, but no corresponding increases in the water vapor. Thus, the high static stability seen by MTP may be confined to altitudes above the aircraft, in which case the aircraft could not have sampled the vortex air at this location, or it may be unrelated to the high PV (and thus the vortex air) seen in the analyses.

Wavelet analysis is a technique that allows investigation into the temporal evolution of a power spectrum. By computing a wavelet power spectrum, one can determine what the dominant wavelengths are and, important for aircraft studies, determine when (or equivalently, where) those wavelengths are dominant. That is, for each wavelength, the wavelet power can be plotted as a time series. Following Torrence and Compo (1998), a Morlet wavelet basis was used to compute the wavelet power spectrum. The data were first detrended and a cosine taper of 10% of the original number of points was applied to ensure periodicity. The wavelet power spectrum was computed for nearly the entire flight. Figures 6–8 show the wavelet power spectra for the INS horizontal wind speed, the ozone, and the PTW temperature measured on board the WB57F for the northernmost section of flight (and so no "cone of influence", or region where edge effects occur, exists in these plots), corresponding to Figure 2. A lag-1 autoregressive process was used to model a red noise spectrum with the same lag-1 autocorrelation as the observations (Gilman et al.

1963). The 95% significance level using this red noise spectrum is also contoured in Figures 6–8 and shows regions where the power is significantly high. The wind speed, temperature, and ozone are all 1 Hz data, so the Nyquist period is 2 s. The nominal aircraft speed of 200 m $s^{-1}$ was used to convert frequencies to wavelengths using Taylor's hypothesis.

The wind speed power spectrum (Figure 6) shows significantly high power at a period of about 10 s (2 km wavelength) throughout the time period shown. At Points "D" and "I", where gravity wave activity occurred, there is high power from 2 to 20 s. In contrast, at other times the high power is concentrated only around 10 s. Though structure is evident at larger periods, none is significantly high at the 95% level.

The ozone wavelet power spectrum (Figure 7) shows peaks in power at several times. These peaks are generally spread throughout the low periods, up to 200 s (40 km wavelength), and are not as widespread in time nor as concentrated in the 10 s period as the power in the wind speed spectrum. The regions of the large gravity waves, Points "D" and "I", show high power, but other regions also show high power, for example, before 63,000 s and between Points "E" and "F". MTP shows a smaller gravity wave just before 63,000 s primarily below the aircraft altitude, while between Points "E" and "F" an increase in the static stability can be seen as the isentropes become closer together; these features may be related to the high ozone power seen there.

Figure 8 plots the temperature wavelet power spectrum. Significantly high power is evident at Points "D" and "I", the large gravity waves, for periods from 2 to 1000 s and higher. Another notable feature of the temperature spectrum is the presence of two times of concentrated 10 s power at Points "A" and just before 63,000 s. These are also evident in the pressure wavelet power spectrum (not shown), and correspond to the concentrated increase in power in the wind speed power spectrum, though in contrast to the temperature and pressure the wind speed power spectrum shows clear evidence of this behavior throughout much of the flight (and the high power shifts to slightly lower periods, perhaps in response to a decrease in altitude). These two times of high temperature power occur during level flight (in pressure). The oscillations of pressure lead temperature oscillations by 30–50°, and lead wind speed oscillations by 120°. Though pressure leading wind speed could be explained by a lack of time synchronization between PTW and INS, both pressure and temperature are measured by PTW. On no other WAM flight do these 10 s power anomalies appear in temperature and pressure; on the April 9 flight there is a suggestion of concentrated 10 s power in the wind speed, but it is less clear than on April 11. The aircraft's autopilot operates with a 1 Hz response, and so is not likely to be the explanation. Further investigation is required to explain these features.

## 3. Model Description

MM5 was used to simulate the observed gravity waves. MM5 solves the primitive equations governing the motion of the atmosphere in full three-dimensional form and incorporates all known major physical parameterizations needed, including boundary layer processes, radiation, and moist processes. MM5 is a nonhydrostatic, compressible grid point model and uses a terrain-following coordinate in the vertical. In MM5 the prognostic variables are wind, temperature, pressure perturbation, and several moisture variables.

In this study, three interactive, nested domains were used with grid spacings of 60, 20, and 6.67 km. The inner two domains are shown in Figure 1; the outermost domain extends from approximately the dateline to the eastern US and from 15 to 65°N. The innermost domain is shown in Figure 3 along with the topography used; the original resolution of the topography was 1 km. The model was configured with 41 vertical levels, at about 700 m vertical grid spacing, and the model top was located at 30 hPa. The time step was set to 100 s. A radiative upper boundary condition was used at the top of the model to reduce reflection of waves. The Hong and Pan (1996) planetary boundary layer parameterization, used in the Medium-Range Forecast (MRF) model at the National Centers for Environmental Predication (NCEP), was specified.

The model was initialized at 00 UTC on April 11 using ECMWF analyses winds and temperatures as well as available radiosonde observations. The analyses have a horizontal resolution of 1.25° (T106), a model top of 10 hPa, and are available every six hours. ECMWF analyses also provided the boundary conditions during the MM5 integration. The model was integrated for 18 hours. MM5 accurately simulated the large scale features seen in the analyses, such as the movement of the vortex filament at 450 K and the position of 500 hPa heights.

## 4. Model Results

Figure 9 shows the MM5 output interpolated to the WB57F flight track and for the same altitude region as in Figure 5. The MM5 output has been interpolated at each location to the aircraft observation time, using the model end time of 18 UTC for aircraft times later than this. The MM5 $\theta$ surfaces show a breaking gravity wave at Points "D" as indicated by the spreading of the $\theta$ surfaces and nearly vertical contours at aircraft altitudes. The breaking wave at Point "I" is stronger in the MM5 output than at Point "D", with closed contours of potential temperature appearing. Both events have limited vertical extent. In contrast, the MTP data indicate large vertical extent of the breaking waves, possibly owing to the real wave breaking only enough to

allow further vertical propagation (that is, the real waves are saturated above the initial breaking altitude). Furthermore, MM5 may be unable to resolve the small-scale gravity waves that could be contributing to the breaking at different altitudes.

The MM5 output reveals weaker stability compared to the MTP; while the 420 K isentrope is located in roughly the same location in both data sets, about 90-100 hPa, the 500 K isentrope is at a much higher altitude in the MM5 output (50 hPa) than in the MTP observations (55-60 hPa). At flight altitude, the MM5 temperatures are too cold by 10–20 K compared to the MTP temperatures. The small scale structure of the $\theta$ surfaces in the MTP data is not evident in the MM5 output. Some of this smoothness is due to the relatively large spatial scale of MM5. At a grid spacing of 6.67 km, the MM5 data correspond to a time of 33 s in the figure. Small scale fluctuations cannot be resolved by the MM5 domain, and the smaller gravity waves that disturb the atmosphere at small scales are not generated in MM5. However, the figure appears too smooth even at scales larger than 20 km (100 s). This is analyzed further in section 5 below.

Model-generated vertical velocities and potential temperatures are shown in Figure 10 along a vertical cross-section oriented perpendicular to the flight track across the Laramie Mountains (southwest-northeast) (Point "D"). Alternating positive and negative vertical velocities propagating upward from the mountain crest are evidence of a vertically propagating gravity wave. At 70–80 hPa, near aircraft altitude, the $\theta$ surfaces show evidence of spreading, indicating convective instability and breaking. In addition, the vertical velocity perturbations do not appear above this altitude.

The vertical cross-sections of MM5 vertical velocities and isentropes at 18 UTC over the Bighorn Mountains (Points "H" and "I") are plotted in Figure 11, analogous to Figure 10. In addition to the location of the northbound aircraft location (cross), the southbound aircraft location is indicated (dot). The time of 18 UTC was chosen as the aircraft passed over this location about 12 minutes before (northbound) and 18 minutes after (southbound), and 18 UTC was the end of the model integration; the model output did not indicate much change in the wave structure from 17 to 18 UTC.

Figure 11 reveals that the aircraft flew northbound to the west of the region of the breaking gravity wave, and on the southbound section the aircraft was at the lower altitude of the breaking gravity wave. According to the MM5 output, if the aircraft had flown southbound at slightly higher altitudes, e.g., at 80 hPa instead of 90 hPa, it would have encountered more severe turbulence than was predicted over the Laramie Mountains.

Analysis of model output from previous times reveals that the gravity waves began at 6 UTC on April 11 and continued through the end of the model run at 18 UTC. The gravity waves occurred in conjunction with an increase in the 700 hPa wind upstream from the mountains (Figure

3). Gravity wave propagation is evident throughout the innermost model domain in close connection with the topography.

While MM5 accurately models the long vortex filament seen in Figure 1, the high PV blob over Wyoming does not appear as clearly defined in the model output as in the ECMWF analyses. There are anomalously high and low PV patches throughout the innermost model domain, and these are uncorrelated with gravity wave propagation. Thus, the gravity waves in MM5 do not require the increased static stability possibly associated with a blob of high PV air in order to propagate or break.

## 5. Scale Analysis

A comparison of Figures 5 and 9 reveals that the MM5 data appear to be much smoother than the MTP contours, even at much larger scales than the MM5 grid spacing of 6.67 km (corresponding to 33 s of aircraft time). To investigate this, spectral analysis of the model and observations is presented in this section as well as the calculations of scaling properties.

### a. Spectral Analysis

The MM5 output temperatures and horizontal winds at 1720 UTC were interpolated to the WB57F flight track and altitude from the edge of the model domain (61,500 s) to the turnaround (most northern) point (65,000 s). Interpolation to each 1 s (0.2 km) aircraft point resulted in a decrease in power at the smallest wavelengths from 10-40 km compared to a spectrum computed at a horizontal grid spacing similar to the domain, so it was decided to interpolate the model data without changing the original model grid spacing significantly. Since the flight track is angled at 45° to the model domain, the horizontal spacing was chosen to be $\Delta x / \cos 45° = 9.4$ km, where $\Delta x$ was the grid spacing of the inner domain. The power spectrum was then computed for the detrended model data and observations; a cosine taper was applied to both ends using 10% of the points to ensure periodicity. Using Taylor's hypothesis and the aircraft speed of 200 m $s^{-1}$ the times of aircraft observations were converted to distance.

The WAM observations and interpolated MM5 model output are shown in Figures 12a (temperature) and 13a (wind speed). The corresponding power spectra $E(k)$, where $k$ is the scale, are shown in Figures 12b and 13b. For both variables the power of the observed quantity exceeds the model power all almost all wavelengths. At wavelengths less than 50 km, well above the Nyquist wavelength for the model data (18 km) and in wavelength regions that one would expect

MM5 to model accurately, the model power is less than the observed power by a factor of 10 to 100.

Interpolation, even to comparable grid spacings, smoothes the data and reduces the power at the smallest wavelengths. This may explain some of the differences between the model and observed power at the smallest wavelengths, but the large differences at larger (e.g., 50 km) wavelengths may be due to inaccurate modeling of atmospheric motions by MM5. For example, the substantial increase in temperature of 10 K from 0 to 200 km in Figure 12a and subsequent sharp decrease is missing from the MM5 output. Similarly, the large scale wind speed oscillations of 20 m $s^{-1}$ seen in the observations throughout the region do not occur in the MM5 data (Figure 13a).

Also shown in Figures 12b and 13b is the power law scaling exponent $\beta$, where

$$E(k) \propto k^{-\beta}. \qquad (3)$$

For the aircraft observations, $\beta$ was computed over the range of scales of the interpolated MM5 output (Table 1). For the PTW temperature, there appears to be a scale break at about 10 km: the power spectrum flattens out slightly at the largest scales, where $\beta$ is computed, compared to smaller scales. The power spectrum also flattens out somewhat at the smallest scales, which is indicative of white (instrumental) noise (Davis et al. 1996). For temperature, $\beta$(PTW) is less than $\beta$(MM5), indicating that for MM5 the smallest scales are not contributing as much as in the real atmosphere. Similarly, for wind speed $\beta$(MM5) is less than $\beta$(INS).

A striking feature of the INS wind speed spectrum is the large increase in power seen around 2 km (corresponding to 10 s). A small peak in the PTW temperature power spectrum is also evident, though its magnitude and width are much less than seen in the wind speed spectrum. This feature has been discussed above and can be seen in the wavelet power spectra (Figures 6 and 8).

b. Scale Analysis

Following Davis et al. (1994), we calculated two properties of multiscaling for the temperatures and horizontal wind speeds observed by the aircraft and modeled by MM5. The first uses structure functions to determine persistence, and the second measures intermittency. The MM5 data were interpolated to the WB57F flight track as described in Section 5a above.

1. *Structure Functions*

Structure functions of each variable were computed and are measures of the amount of persistence (smoothness) or antipersistence (roughness) of the data. A family of exponents $H(q)$ was calculated, where $q$ is the statistical moment. $H_1$ (i.e., $H(q)$ where $q = 1$) has been used by various authors (Davis et al. 1994, 1996, 1997; Marshak et al. 1997) as a qualitative indicator of persistence. $H_1$ ranges from 0 (antipersistence, stationarity, neighboring points are more likely to be anticorrelated; white noise is an example) to 1 (persistence, nonstationarity, neighboring points are more likely to be correlated; a line with a nonzero slope is an example). Following the notation of Davis et al. (1994), we define $\varphi(x)$ to be the data set we are interested in (temperature or wind speed from WAM or MM5). The scaling exponent $\beta$ is used to test the stationarity of $\varphi(x)$. If the data set is nonstationary ($\beta > 1$) with stationary increments ($\beta < 3$), as are all four data sets of interest (Table 1), then we can define

$$\Delta\varphi(r;x) = \varphi(x + r) - \varphi(x), \qquad 0 \le r \le L, \qquad 0 \le x \le L - r \tag{4}$$

where $r$ is the interval length and $L$ is the length of the data set. Because these increments are stationary, we can average over $x$ ($\Delta\varphi(r;x) = \Delta\varphi(r)$). Taking absolute moments of $\Delta\varphi(r)$, if the data set is scale invariant then

$$\left\langle \left|\Delta\varphi(r)\right|^q \right\rangle \propto r^{\zeta(q)} \tag{5}$$

where $\left\langle \left|\Delta\varphi(r)\right|^q \right\rangle$ is termed the $q$th order structure function. The family of exponents $H(q)$ can be defined as

$$H(q) = \frac{\zeta(q)}{q} \tag{6}$$

If $H(q)$ varies with $q$, then the data set is called "multifractal" or "multiscaling".

Figure 14 shows the structure functions of all four data sets on a log-log plot for $q = 1$. $H_1$ is the slope of the linear least squares fit and is shown in Table 1. $H_1$ using MM5 temperature is 0.64 indicating some persistence in the data; this smoothness can be seen in the temperature in Figure 12a. Using the entire range of scales present in the PTW temperature, $H_1 = 0.54$. However, using only the range of scales available to MM5, $H_1 = 0.36$. Thus, over wavelengths greater than 9.4 km, the PTW temperature is more antipersistent (or anticorrelated) than the MM5 temperature. There appears to be a scale break at roughly 10 km, with higher $H_1$ for the smaller scales.

Similar results occur for the comparison between INS and MM5 wind speed. The $H_1$ computed for all INS scales is more similar to that computed only for the MM5 scales, however (0.25 compared to 0.29). The scatter in the points about the $H_1$=0.25 line suggests that wind speed may not be a scale invariant process across all scales. In particular, there are large deviations from the least squares fit around $\log_{10}$(2 km)=0.3, corresponding to the peak at 2 km in the Fourier and wavelet power spectra.

Since $\beta = 2H_2 + 1$ (Davis et al. 1994), we can use the results from Figures 12b and 13b to compare with the calculated $H2$ over the MM5 range of scale. Large differences occur only for the INS wind speed (Table 1); together with the scatter of points around the least squares fitted line this may indicate the lack of scale invariance of the INS wind speed even at the largest scales.

All four data sets are multifractal since the $H(q)$ for each were not constant when varying $q$ (Table 1).

2. *Intermittency*

Intermittency was also calculated and measures how sparse or spiky the data set is. Analogous to $H_1$, $C_1$ is a measure of the intermittency of the data set. Extremes range from $C_1 = 0$ for white noise to $C_1 = 1$ for functions such as the Dirac delta function and the Heaviside step function (Marshak et al. 1997). To calculate $C(q)$, we begin with a nonstationary data set with stationary increments and determine the range of scales, from $\eta$ to $R$, where scale invariance occurs. For the four data sets of interest, all MM5 scales were used ($k$ > 9.4 km). Then, at the smallest scale $\eta$ (9.4 km) we define

$$\varepsilon(\eta;x) = \frac{\left|\Delta\varphi(\eta;x)\right|^m}{\left\langle\left|\Delta\varphi(\eta;x)\right|^m\right\rangle} \qquad 0 \le x < L - \eta \tag{7}$$

Following Davis et al. (1994), we take $m$ = 1. The average over a particular scale $r$ is then computed:

$$\varepsilon(r;x) = \frac{1}{r}\int_x^{x+r} \varepsilon(\eta;x')\,dx', \qquad \eta < r \le L, \qquad \eta \le x \le L - r \tag{8}$$

By spatially averaging $\varepsilon(r,x)$, we can seek a power-law dependence of $\varepsilon(r)$ on $r$ for a given order $q$:

$$\left\langle \varepsilon(r)^q \right\rangle \propto r^{-K(q)} \tag{9}$$

Similar to the calculation of $H(q)$,

$$C(q) = \frac{K(q)}{q - 1} \tag{10}$$

$C_1$ is computed following l'Hospital's rule as the (numerical) derivative of $K1$.

Using the MM5 wind speed and temperature resulted in similar values for $C_1$, about 0.09 (Table 1). The WAM wind speed and temperature observations were also similar, $C_1 = 0.05$, but lower than the MM5 values. All four data sets, therefore, have low intermittency; this can be seen as the lack of large amplitude spikes in the data sets. As an example of results from another geophysical data set, Marshak et al. (1997) reported $C_1$ values ranging from 0.03 to 0.15 for liquid water content in marine stratocumulus clouds.

## 6. Conclusions

A flight during the WB57F Aerosol Mission revealed several interesting dynamical features in the stratosphere on April 11, 1998. From the observations on board the aircraft, comparisons with HALOE profiles, and trajectory modeling, it appears the WB57F flew through air that originated at the edge of the polar vortex. Gravity waves were observed in the lower stratosphere during the flight over the Laramie and Bighorn Mountains. Severe turbulence was reported by the pilot, and instruments measured large fluctuations in horizontal wind speed and direction and an increase in the variability of ozone in the vicinity of the wave. In addition, potential temperature surfaces as measured by MTP were nearly vertical at the locations of the turbulence. Wavelet power spectra of wind speed, temperature, and ozone show significant power (at the 95% level) in the regions of the gravity wave.

A high spatial resolution mesoscale atmospheric model (MM5) was run to simulate the gravity wave. Though the temperatures of the model were too low compared with those measured by MTP, the model predicted the location and altitude of the gravity waves fairly well. Evidence of the wave structure is apparent from the vertical velocity perturbations and the potential temperature characteristics in the model output. The strength of the breaking wave over the Laramie Mountains appeared less in the model output than reported by the pilot and observed on board the aircraft, which could be due to the lack of small-scale gravity waves in the model or the timing of the increase in the surface level wind. Analysis of the event over the Bighorn Mountains indicated that more severe turbulence may have been encountered by the aircraft had it flown slightly higher on the southbound section of flight.

The blob of high PV air seen in the ECMWF analyses over Wyoming was a result of an increase in the wind shear, and only a slight change in the static stability. Furthermore, the gravity waved produced by MM5 were uncorrelated with regions of high PV in the model. Therefore, it appears that while the vortex air sampled by the aircraft could have modified the atmospheric conditions somewhat, the model results indicate that the gravity waves would have occurred (and broken) in the lower stratosphere even in the absence of the vortex air.

Scale analysis of the observations and MM5 output of temperature and horizontal wind speed indicate that MM5 may not be correctly modeling small scale motions in the atmosphere. Power spectra show that MM5 data have substantially less power at scales around 50 km, well above the Nyquist wavelength, relative to the larger scales. This smoothness in the MM5 data compared to the observations can be seen by comparing the potential temperature surfaces along the flight track from MTP and MM5 (Figures 5 and 9) and in the wind speeds and temperatures (Figures 12a and 13a); by noting the larger $\beta$ for the MM5 output (Table 1), indicating less small scale activity compared to the larger scales; and by comparing the calculated persistence measures $H_1$ (Table 1), which are higher (more persistent, or more correlated) for the MM5 output.

This study demonstrates the capability of MM5 to simulate gravity waves, though the simulations are not perfect. The MM5 results were verified using aircraft observations, increasing the confidence of using MM5 for additional case studies where gravity waves play an important role. This study shows that MM5 may be able to predict breaking gravity waves and so could be utilized for avoiding turbulence during aircraft flights.

Acknowledgements. We wish to thank the MM5 group at NCAR/MMM for assistance running the model; Steve Reid and ECMWF for the ECMWF analyses as well as for assistance with the trajectory modeling; and Bruce Gary, Joan Alexander, Tom Warner, Bob Sharman, and Hsiao-ming Hsu for helpful discussions. This work was supported in part by a grant of HPC resources from the Arctic Region Supercomputing Center. Dan Murphy is gratefully acknowledged for the use of the PALMS data. Wavelet software was provided by C. Torrence and G. Compo, and is available at http://paos.colorado.edu/research/wavelets.

## References

Bacmeister, J. T., M. R. Schoeberl, L. R. Lait, P. A. Newman, and B. Gary, 1990: ER-2 mountain wave encounter over Antarctica: Evidence for blocking. *Geophys. Res. Lett.*, **17**, 81-84.

Denning, R. F., S. L. Guidero, G. S. Parks, and B. L. Gary, 1989: Instrument description of the airborne Microwave Temperature Profiler. *J. Geophys. Res.*, **94**, 16,757-16,765.

Davis, A., A. Marshak, W. Wiscombe, and R. Cahalan, 1994: Multifractal characterizations of nonstationarity and intermittency in geophysical fields: Observed, retrieved, or simulated. *J. Geophys. Res.*, **99**, 8055-8072.

Davis, A., A. Marshak, A., W. Wiscombe, and R. Cahalan, 1997: Scale invariance in liquid water distributions in marine stratocumulus. Part I: Spectral properties and stationarity issues. *J. Atmos. Sci.*, **53**, 1538-1558.

Gilman, D. L., F. J. Fuglister, and J. M. Mitchell, 1963: On the power spectrum of "red noise". *J. Atmos. Sci.*, **20**, 182-184.

Grell, G. A., J. Dudhia, and D. R. Stuaffer, 1994: A description of the fifth-generation Penn State/NCAR mesoscale model (MM5). *Tech. Note 398*, 121 pp., National Center for Atmospheric Research, Boulder, CO.

Holton, J. R., 1992: An Introduction to Dynamic Meteorology, Academic Press, 511 pp.

Hong, S.-Y., and H.-L. Pan, 1996: Nonlocal boundary layer vertical diffusion in a medium-range forecast model. *Mon. Wea. Rev.*, **124**, 2322-2339.

Leutbecher, M., and H. Volkert, 1996: Stratospheric temperature anomalies and mountain waves: A three-dimensional simulation using a multi-scale weather prediction model. *Geophys. Res. Lett.*, **23**, 3329-3332.

Marshak, A., A. Davis, W. Wiscombe, and R. Cahalan, 1997: Scale invariance in liquid water distributions in marine stratocumulus. Part II: Multifractal properties and intermittency issues. *J. Atmos. Sci.*, **54**, 1423-1444.

Murphy, D., T. T. Thompson, and M. J. Mahoney, 1998: In situ measurements of organics, meteoritic material, mercury, and other elements in aerosols at 5 to 19 kilometers. *Science*, **282**, 1664-1669.

Table 1. Scaling properties computed using the PTW temperature and INS wind speed observations during WAM and the MM5 temperature and wind speed interpolated to the WAM flight track at 9.4 km grid spacing. Results from the WAM observations have been computed using only the range of scales available in the interpolated MM5 data. $H_1$ indicates persistence; $C_1$ indicates intermittency; both range from 0 to 1. Note that if a process is scale-invariant and is nonstationary with stationary increments, then $\beta = 2H_2 + 1$. Multifractality or multiscaling is indicated by the nonconstant values of $H_1$, $H_2$, and $H_6$.

| Data set | $H_1$ | $H_2$ | $H_6$ | $\beta$ | $2H2 + 1$ | $C_1$ |
|---|---|---|---|---|---|---|
| PTW Temperature | 0.36 | 0.33 | 0.23 | 1.59 | 1.66 | 0.05 |
| MM5 Temperature | 0.64 | 0.58 | 0.50 | 2.00 | 2.16 | 0.09 |
| INS Wind Speed | 0.29 | 0.25 | 0.15 | 1.83 | 1.5 | 0.05 |
| MM5 Wind Speed | 0.58 | 0.53 | 0.45 | 2.05 | 2.06 | 0.09 |

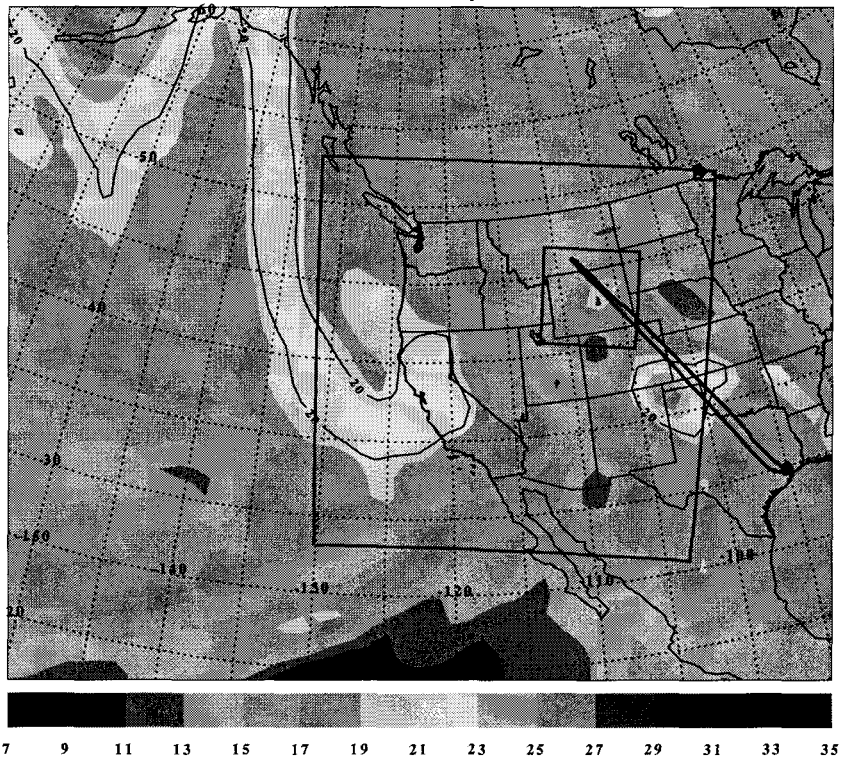


Figure 1. ECMWF potential vorticity (PV; PV units where 1 PV unit = $10^{-6}$ K $m^2$ $kg^{-1}$ $s^{-1}$) over the eastern Pacific and western United States on the $\theta$ = 450 K surface for April 11, 1998, at 18 UTC. Boxes indicate inner two domains used in MM5 model run. WB57F Aerosol Mission flight track originating in Houston, Texas (30°N, 95°W) is shown by the solid curve. Note the filament of vortex air stretching from Alaska to California and the two blobs of high PV air intersected by the aircraft. The northern one was sampled by the aircraft, while the aircraft was lower than the southern blob.

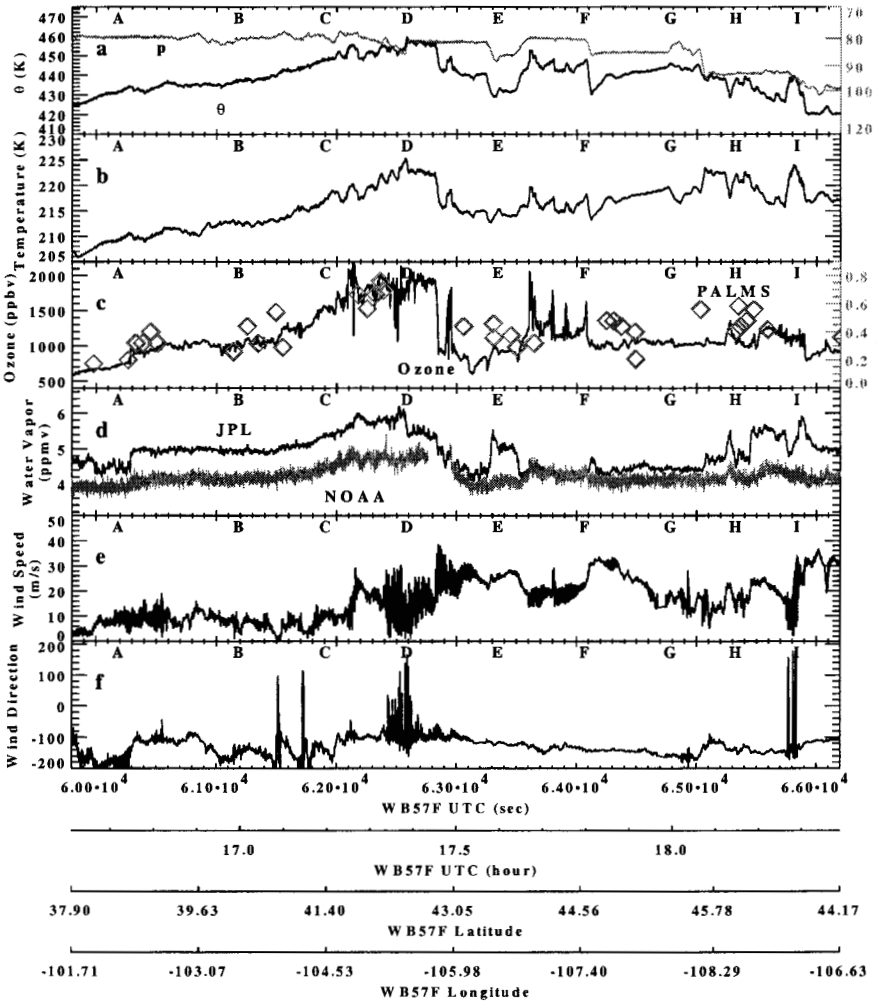


Figure 2. Traces of aircraft observations on April 11, 1998 for the northernmost section of flight. (a) Pressure (black curve) and potential temperature (gray curve) and (b) temperature measured by PTW; (c) ozone (solid curve) and PALMS fractions of aerosols containing meteoritic material (diamonds); (d) water vapor measured by the JPL TDL (black curve) and NOAA Lyman-α (gray curve) instruments; (e) wind speed and (f) wind direction from the Inertial Navigation System. Letters "A" through "I" correspond to points located on map in Figure 3.


Figure 3. Map of northernmost section of WB57F flight track on April 11, 1998. Contours of elevation (m) used in the MM5 simulation are plotted with an interval of 250 m. Wind barbs indicate direction and speed (m/s) of 700 hPa winds from ECMWF analyses at 18 UTC on flight day. Points "D" (Laramie Mountains) and "I" (Bighorn Mountains) are the locations of the major gravity waves.

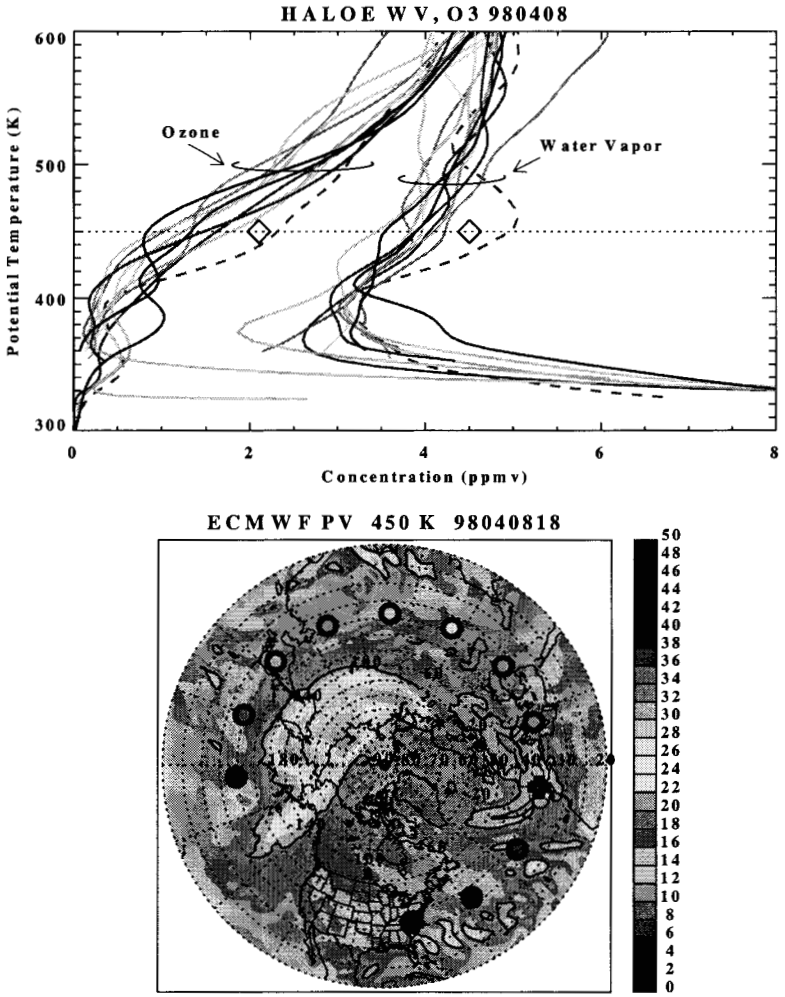


Figure 4. (a) HALOE ozone and water vapor profiles from April 8, 1998. Diamonds show aircraft observations of water vapor and ozone adjusted to HALOE values. (b) Map of locations of HALOE profiles and ECMWF potential vorticity (PV units) on April 6, 1998 at 18 UTC. 20 PV unit contour is drawn to approximate the vortex edge. The HALOE profile sampling vortex air at 10°W is indicated by the blue dashed curve in (a) and the blue plus in (b); the other profiles sampled midlatitude air and are indicated by colored solid curves (a) and circles (b).

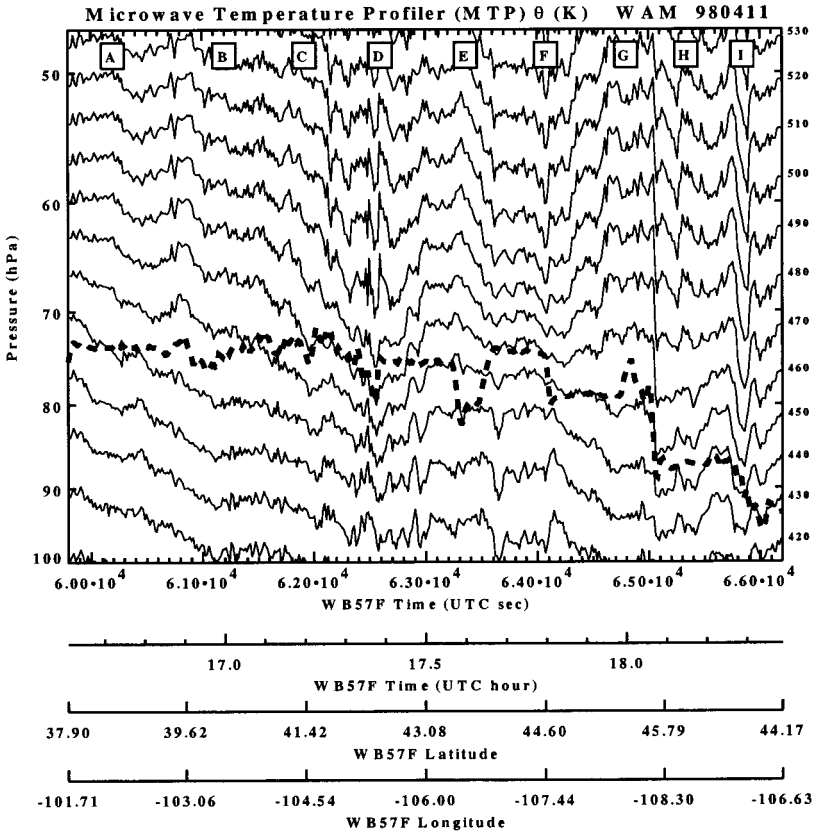


Figure 5. Potential temperature surfaces (K) from Microwave Temperature Profiler (MTP) flying on northbound WB57F on April 11, 1998. Contour interval is 10 K. Letters "A" through "I" correspond to points located on map in Figure 3. Flight altitude is plotted as dashed curve. Major gravity wave events are located at "D" and "I".

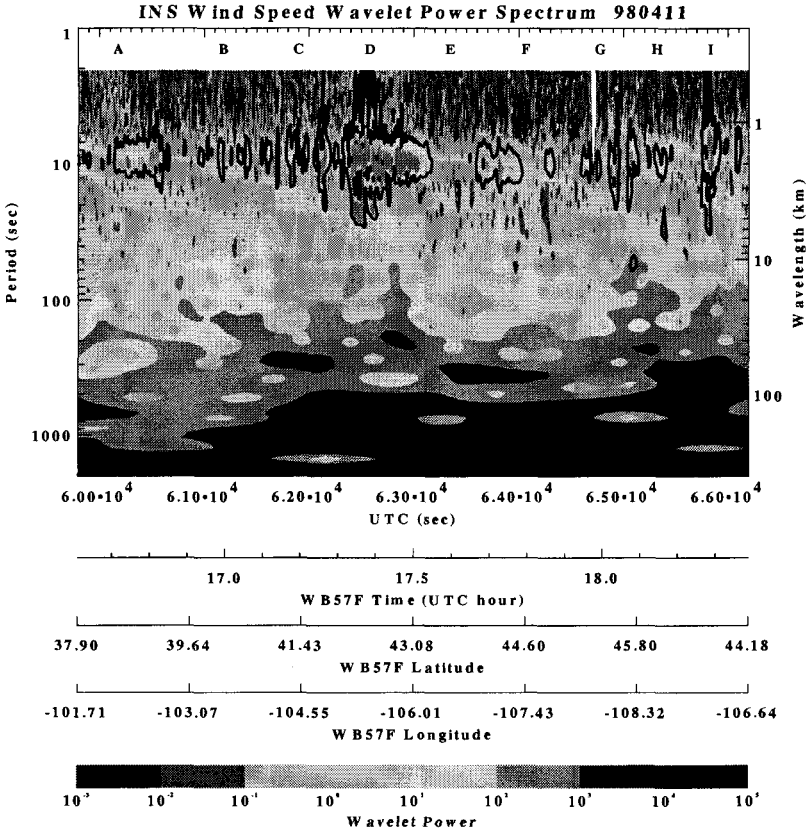


Figure 6. Section of INS wind speed wavelet power spectrum corresponding to Figure 2. Thick contour indicates 95% significance level for a red noise spectrum computed using a lag-1 autoregressive model. Periods were converted to wavelengths using aircraft speed of 0.2 km $s^{-1}$. Major gravity waves occur at Points "D" and "I".

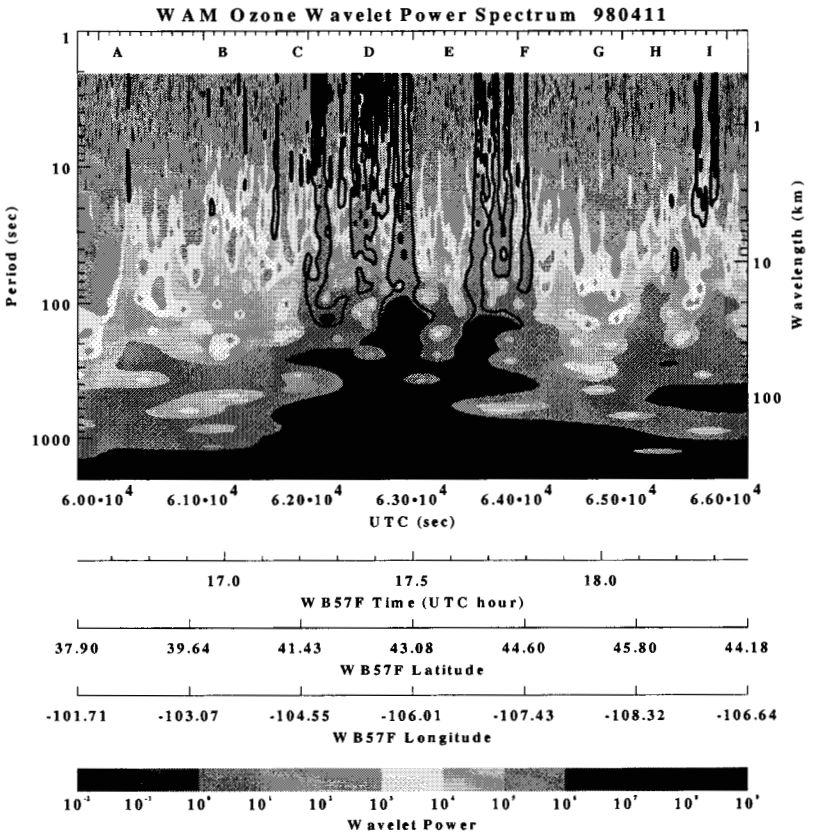


Figure 7. Ozone wavelet power spectrum. See Figure 6 for details. Note lack of concentrated power at 10 s that is seen in the wind speed wavelet.

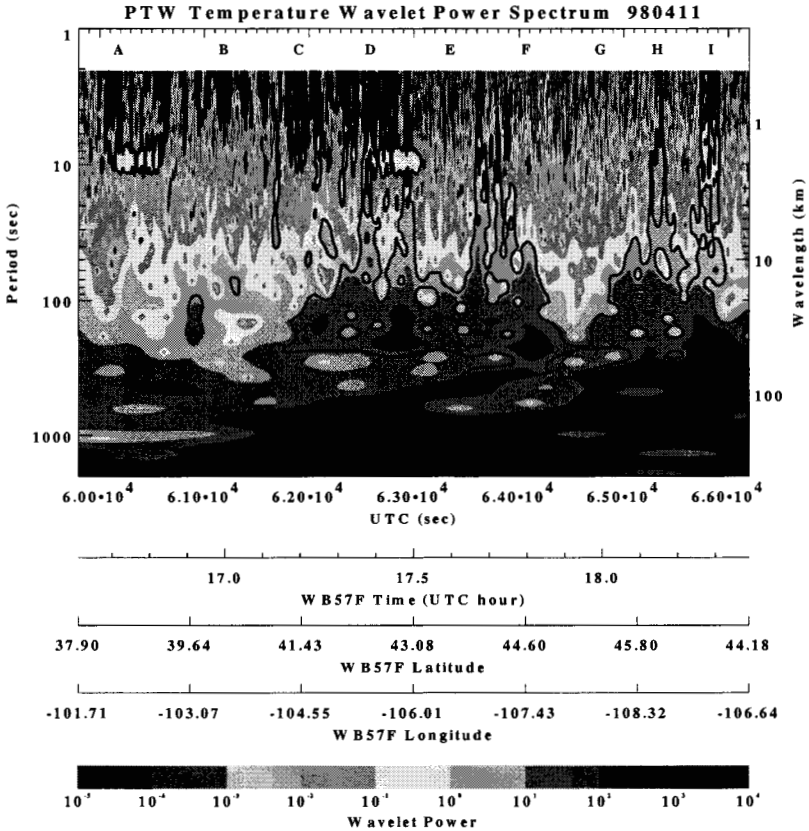


Figure 8. PTW temperature wavelet power spectrum. See Figure 6 for details. Some concentrated power at 10 s appears, but is not as prevalent as for wind speed.

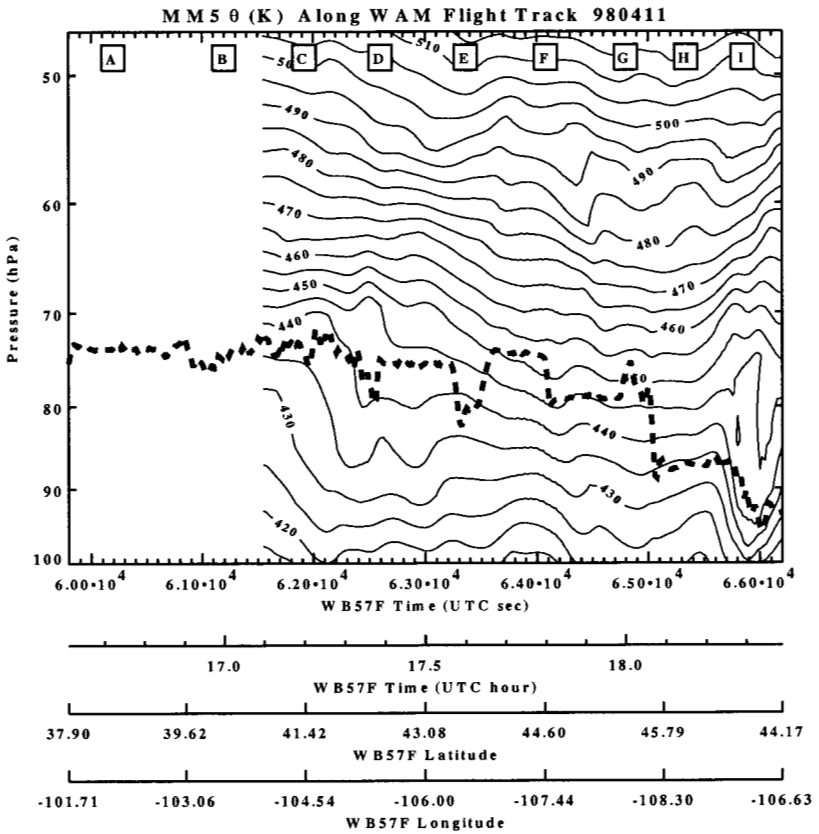


Figure 9. Same as Figure 5 but for MM5 model potential temperatures interpolated to WB57F flight track and times. Model domain begins at 61,500 s. Contour interval is 5 K.

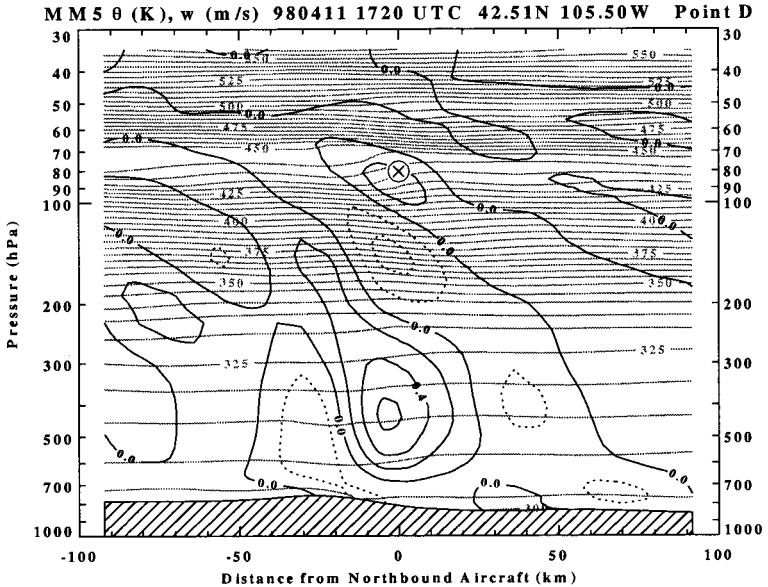


Figure 10. Vertical cross-section of MM5 vertical winds (thick curves; dotted indicate negative values; m/s) and potential temperature (gray curves; K) from model time 1720 UTC on April 11, 1994, at 42.5°N, 105.5°W (Point "C" in Figure 3). Data are plotted perpendicular to flight track and relative to aircraft location on ground; west is to the left. Hatched region indicates topography. Aircraft location indicated by cross.

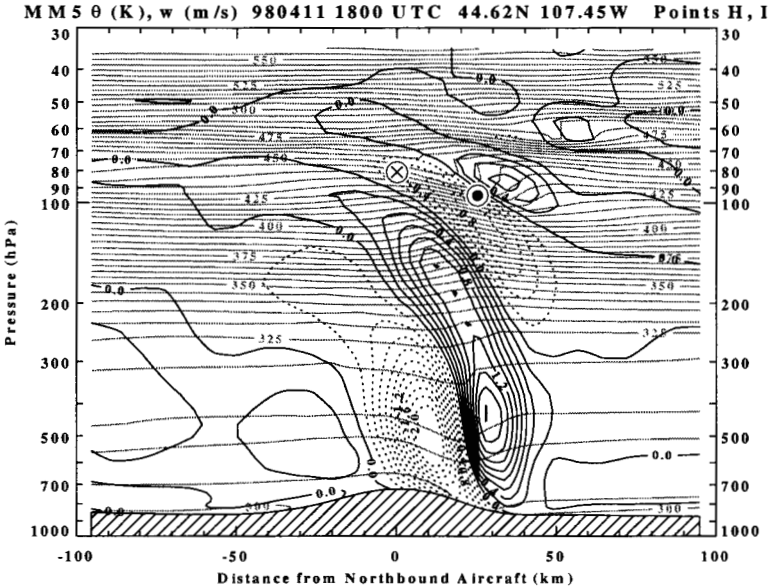


Figure 11. Same as Figure 7 but at 44.6°N, 107.5°W (Point "H" in Figure 3) and at model time 18 UTC. Northbound aircraft (cross) passed over at 1748 UTC. Southbound aircraft location (Point "I" in Figure 3), at 1818 UTC, indicated by dot to right of northbound aircraft location.

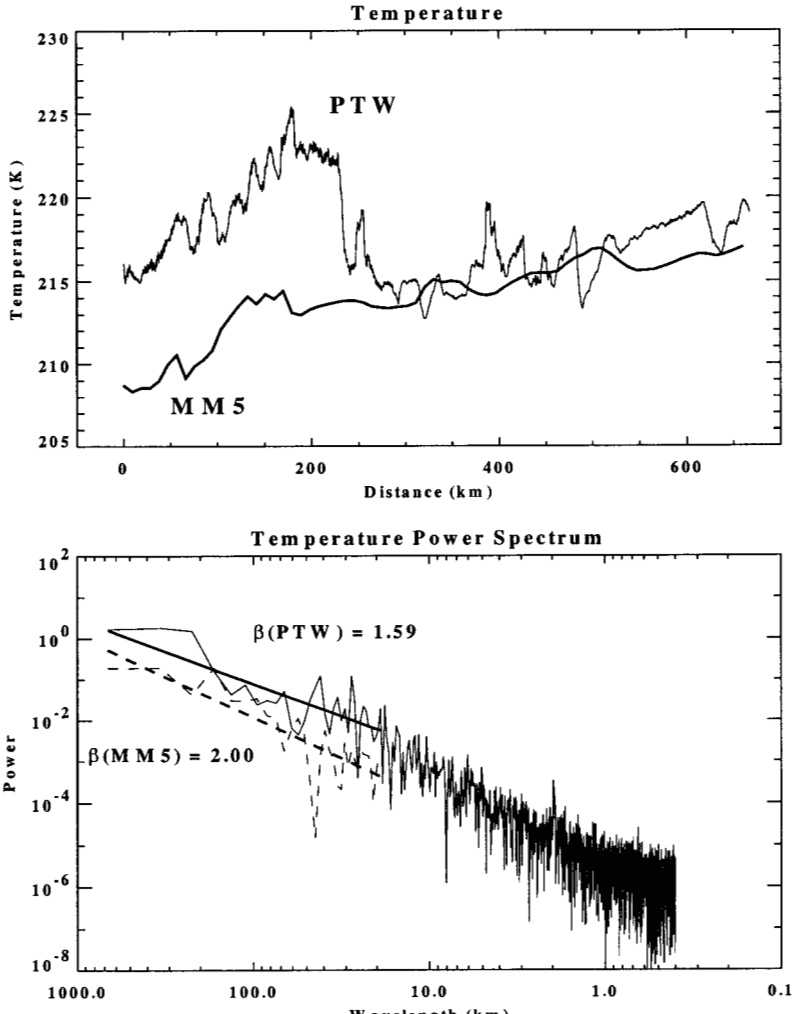


Figure 12. (a) PTW temperature observations and spatially interpolated MM5 temperature at 1720 UTC along WB57F flight track. (b) Power spectrum for PTW (solid curve) and MM5 (dashed curve). Note reduced MM5 power throughout spectrum. Least squares fits to power spectra at MM5 scales also shown along with corresponding $\beta$.

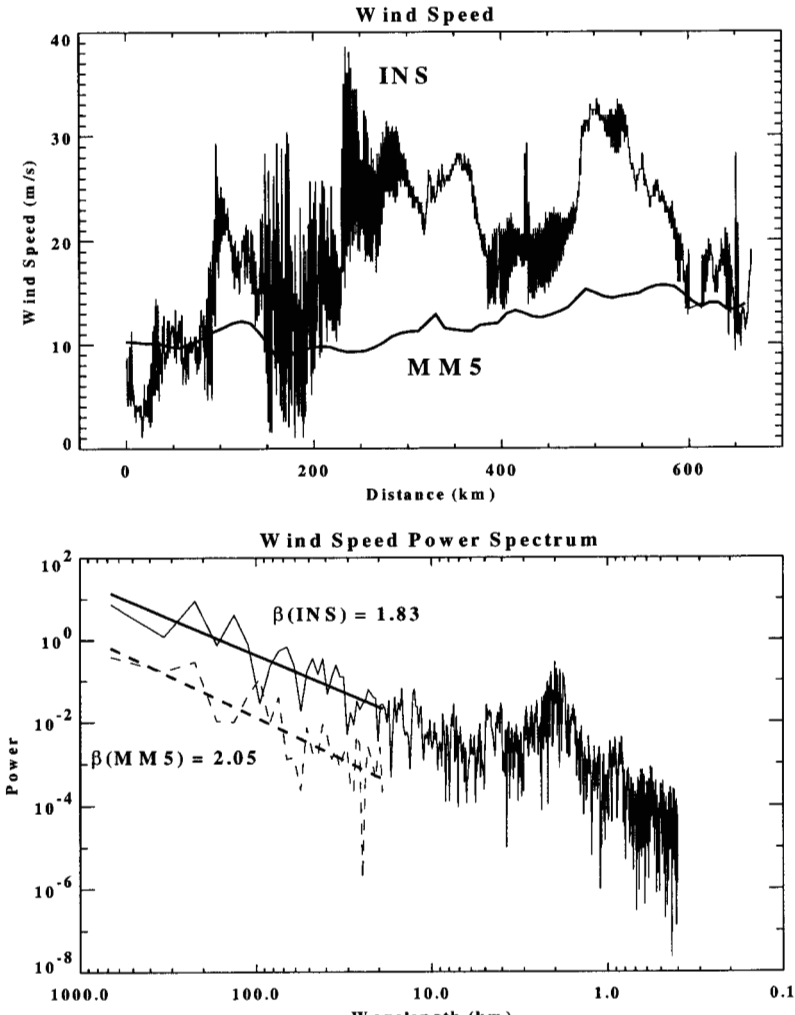


Figure 13. (a) INS and MM5 horizontal wind speed along flight track. (b) Power spectra. See Figure 12 for details.

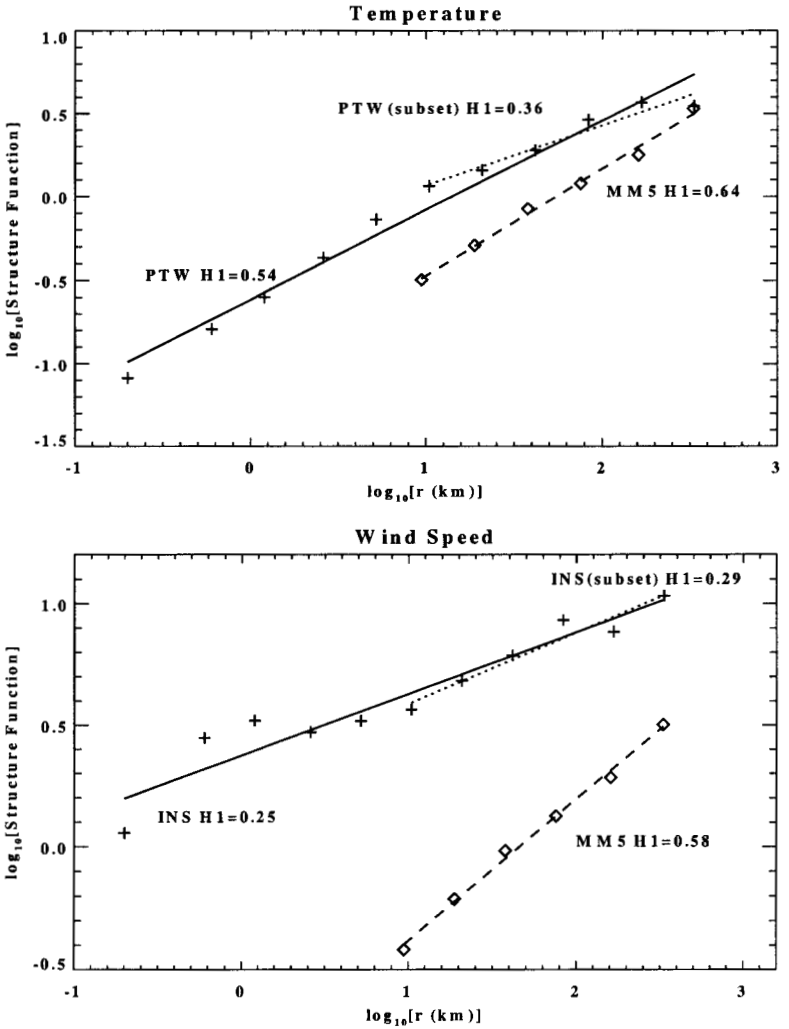


Figure 14. Log-log plot of interval distance versus structure function used in calculation of $H_1$. (a) PTW (plusses; solid line) and interpolated MM5 (diamonds; dashed line) temperatures. (b) INS (plusses) and interpolated MM5 (diamonds) horizontal wind speeds. Least squares fits also plotted. Dotted line indicates fit to observation structure functions using only MM5 scales.